Report no. changed (Mar 2006): SR-371-UU

SACLANT UNDERSEA RESEARCH CENTRE REPORT

SACLANTCEN REPORT
serial no: SR- 371

Formulae for bistatic signal and reverberation

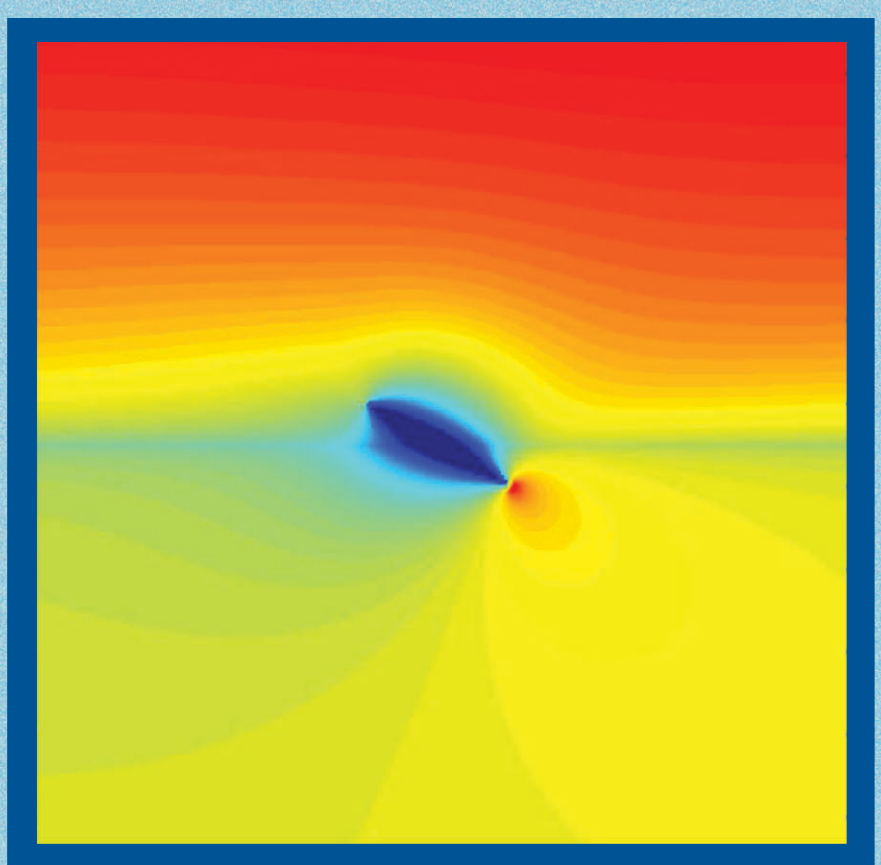

Chris H. Harrison

December 2002

NORTH ATLANTIC TREATY ORGANIZATION ORGANISATION DU TRAITE DE L'ATLANTIQUE NORD

Report no. changed (Mar 2006): SR-371-UU

SACLANTCEN SR-371

Formulae for bistatic signal and reverberation

C H Harrison

The content of this document pertains to work performed under Project 04E of the SACLANTCEN Programme of Work. The document has been approved for release by The Director, SACLANTCEN.

Jan L. Spoelstra
Director

intentionally blank page

SACLANTCEN SR-371

Formulae for bistatic signal and reverberation

C H Harrison

Executive Summary: The value of multistatic sonar is an important issue for ASW. Therefore any method that can help assess the performance of multistatic or bistatic sonars is a potentially useful tool. This report demonstrates that it is possible to obtain closed- form solutions for signal and reverberation in a wide variety of bistatic scenarios including ducts and bottom bathymetry. From this one can immediately obtain signal-to-reverberation-ratio, detection ranges and area coverage. Examples are given for bistatic reverberation with the source and receiver near a shelf at the top of a slope. Results are presented both mathematically and graphically as plots of reverberation *vs* delay time and bearing and reverberation in map projection.

intentionally blank page

SACLANTCEN SR-371

Formulae for bistatic signal and reverberation

C H Harrison

Abstract: This report demonstrates that it is possible to obtain closed-form solutions for signal and reverberation in a wide variety of bistatic scenarios including ducts and bottom bathymetry. These formulae adapt earlier monostatic solutions [SACLANTCEN Reports **SR-356, SR-370, SM-358**]. Examples are given for bistatic reverberation with the source and receiver near a shelf at the top of a slope. Results are presented both mathematically and graphically as plots of reverberation *vs* delay time and bearing and reverberation in map projection

Keywords: Reverberation – SRR – bistatic – bottom slope

Contents

1 Introduction

The performance assessment of bistatic and multistatic sonars relies on the calculation and prediction of reverberation and target echo level. Because there are many permutations of source, receiver and target positions in complex 3D environments fast algorithms have an advantage. Recently some closed-form formulae [1-3] were provided for signal and reverberation in various environments including: isovelocity with a flat bottom, isovelocity with a large range of bathymetries, and a linear refracting duct with a flat or tilted bottom. Each of these can easily be converted into the bistatic case. The reason for this is that, surprisingly, there are no extra integrals to perform. For a point target this is obvious; we simply have outgoing propagation multiplied by propagation back to the receiver at a different location. This is still a closed-form formula. For reverberation we have the same product for each element of area, however *it is not necessary to integrate over these elements* because we actually want the received intensity as a function of delay time and bearing (at the receiver). The elementary area depends on the element of round-trip-travel-time dt which is the pulse length (reciprocal of the bandwidth for FM) and the element of bearing $d\phi$ which is the horizontal beam resolution.

Examples are given for reverberation with the source and receiver on, or in the vicinity of, a shelf at the top of a slope. Results are displayed both as reverberation *vs.* delay time and bearing, and reverberation in map projection.

2
Bistatic geometry

The bistatic derivation below can take any of the earlier fomulae for one-way propagation and scattering [1-3] as their starting point. Thus we could assume isovelocity or a linear sound speed duct with a flat bottom or range-dependent bathymetry. The bistatic derivation does not depend on the form of these equations; the final solution simply includes them. Later we will show examples of bistatic reverberation in a range- and azimuth-dependent environment, but for clarity first we restate the monostatic reverberation result for Lambert's law and a range-independent environment [1]. From Eq. (2.13) in [1] the one-way propagation intensity at a point on the seabed (allowing downward paths only, as discussed in [1]) is

$$I_P = \frac{1}{rH}\int_0^{\theta_c} \exp(-\frac{\alpha\theta^2}{2H} r)\, d\theta = \sqrt{\frac{\pi/2}{H\alpha r^3}}\ \mathrm{erf}(\sqrt{\alpha r/2H}\,\theta_c) \tag{1}$$

If we assume scattering strength to be separable in the two vertical angles and the bistatic angle

$$S_i(\theta_{in}, \theta_{out}, \beta) = S_{in}(\theta_{in})\ S_{out}(\theta_{out})\ S_{bis}(\beta) \tag{2}$$

then for monostatic sonar and Lambert's law we have

$$S = \mu \sin(\theta_{in}) \sin(\theta_{out}) \tag{3}$$

The two-way propagation also separates and we have an identical incoming and outgoing propagation integral

$$P(r) = \frac{1}{rH}\int_0^{\theta_c} \theta\, \exp(-\frac{\alpha\theta^2}{2H} r)\, d\theta = \frac{1}{\alpha r^2}\left(1 - \exp(-\alpha r \theta_c{}^2/2H)\right) \tag{4}$$

and the reverberation is (Eq. (4.6) [1])

$$\begin{aligned} I_R &= P(r)^2\, \mu r \Phi p \\ &= \frac{\mu}{\alpha^2 r^3} \Phi p \left(1 - \exp(-\alpha r \theta_c{}^2/2H)\right)^2 \end{aligned} \tag{5}$$

In going from the monostatic to the bistatic case all that happens is that there is a different range for the incoming (r_r) and outgoing (r_s) propagation and a different scattering area

δA. There are no extra integrations. If we continue to use Eq.(3) for scattering strength there is no dependence on bistatic angle and

$$I_R = P(r_s)P(r_r)\,\mu\,\delta\,A \tag{6}$$

Since we are already given the function $P(r)$ we need to calculate r_s, r_r and δA for a given round-trip delay time and bearing at the receiver. If we know the dependence of scattering strength on bistatic angle β then we can replace Eq. (3) with

$$S = \mu \sin(\theta_{in}) \sin(\theta_{out}) f(\beta) \tag{7}$$

and Eq.(6) becomes

$$I_R = P(r_s)P(r_r)\,\mu\, f(\beta)\delta\,A \tag{8}$$

2.1 Range/Area formulae

We assume the geometry shown in Fig. 1. Source and receiver are separated by distance L, the scattering point is at (r_r ,ϕ) relative to the receiver and a distance r_s from the source.

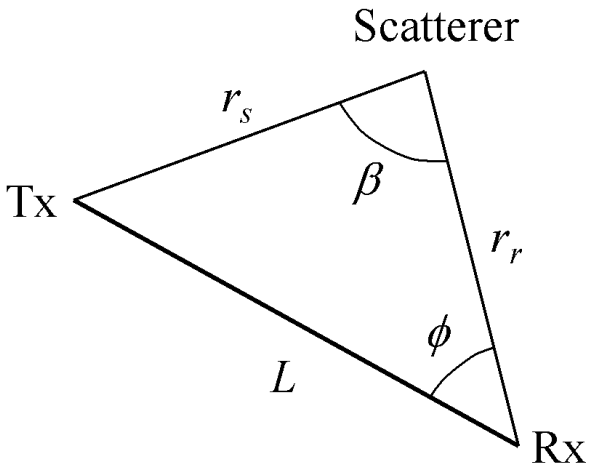

Figure 1 *Bistatic geometry showing source (Tx), receiver (Rx), scatterer, baseline (L) ,ranges (r_s, r_r), bistatic angle (β),and bearing (ϕ).*

Assuming we know the round-trip travel time t and the bearing ϕ we can write two equations for r_s and r_r

$$r_s^{\,2} = r_r^{\,2} + L^2 - 2 r_r L \cos\phi \tag{9}$$

$$ct = r_s + r_r \tag{10}$$

These can be rearranged as

$$r_r = \frac{(ct)^2 - L^2}{2(ct - L\cos\phi)} \tag{11}$$

$$r_s = \frac{(ct)^2 + L^2 - 2Lct\cos\phi}{2(ct - L\cos\phi)} \tag{12}$$

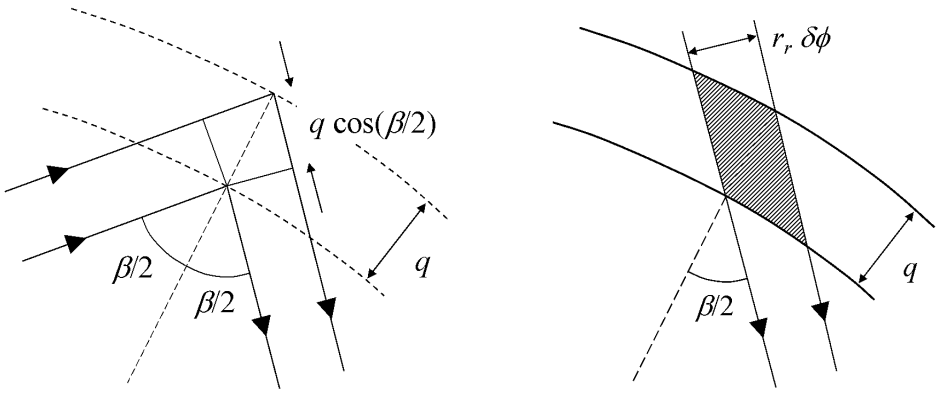

(a) (b)

Figure 2(a) *Geometrical construction for bistatic angle and delay time ellipses, and (b) the area of overlap δA between the equal time ellipses and the beam width radials.*

The geometry to calculate the area is shown in Fig. 2. Regardless of the slightly different delays of each multipath, for a single path we can indicate (Fig. 2(a)) its equal-time ellipse and the ellipse for exactly one pulse length δt later. The local normal to these ellipses bisects the bistatic angle β (a property of ellipses). If we temporarily label the local spatial separation of the ellipses as q we have a path difference

$$c\,\delta t = \delta(r_s + r_r) = 2q\cos(\beta/2) \tag{13}$$

Now in Fig. 2 (b) the desired area is shown to be the overlap of an elementary beam (spatial width $r_r \delta\phi$) and the gap between the ellipses of width q. Thus

$$\begin{aligned}\delta A &= q\, r_r\, \delta\phi / \cos(\beta/2) \\ &= c\,\delta t\, r_r\, \delta\phi / (2\cos^2(\beta/2))\end{aligned} \tag{14}$$

But if we apply the cosine rule to the bistatic angle in Fig. 2(a) we find

$$\cos\beta = \frac{r_s^{\,2} + r_r^{\,2} - L^2}{2r_s r_r} = \frac{(r_s + r_r)^2 - 2r_s r_r - L^2}{2r_s r_r} = \frac{(ct)^2 - L^2}{2r_s r_r} - 1 \tag{15}$$

So

$$2\cos^2(\beta/2) = 1 + \cos\beta = \frac{(ct)^2 - L^2}{2r_s r_r} \tag{16}$$

Substituting this in Eq. (14) the scattering area becomes

$$\delta A = \delta t\ \delta\phi\ \frac{2c\, r_r^{\,2} r_s}{(ct)^2 - L^2} \tag{17}$$

We note incidentally that both the area and the bistatic angle can be written explicitly in terms of t and ϕ.

$$\delta A = c\delta t\ \delta\phi\ \frac{\{(ct)^2 - L^2\}\{(ct)^2 + L^2 - 2Lct\cos\phi\}}{4(ct - L\cos\phi)^3} \tag{18}$$

$$\cos\beta = \frac{2(ct - L\cos\phi)^2}{\{(ct)^2 + L^2 - 2Lct\cos\phi\}} - 1 \tag{19}$$

2.2 Bistatic reverberation

Now returning to Eq. (8) we can write the solution for bistatic reverberation as

$$I_R(\phi, t) = P(r_s)P(r_r)\,\mu\, f(\beta)\delta t\ \delta\phi\ \frac{2c\, r_r^{\,2} r_s}{(ct)^2 - L^2} \tag{20}$$

With Lambert's law the propagation term $P(r)$ can be written as $\alpha^{-1}r^{-2}$ $(1-\exp(-Ar))$ where A is a function of the environment ($A = \alpha\theta_c^{\,2}/2H$), and we obtain

$$I_R(\phi,t) = \left(1-\exp(-A\,r_s)\right)\left(1-\exp(-A\,r_r)\right)\,\frac{2c\,\mu\,f(\beta)\delta t\;\;\delta\phi}{\alpha^2 r_s\{(ct)^2-L^2\}} \tag{21}$$

Substituting for all but the exponents and β we obtain

$$I_R(\phi,t) = \left(1-\exp(-A\,r_s)\right)\left(1-\exp(-A\,r_r)\right)\frac{4c\;\mu\,f(\beta)\delta t\;\;\delta\phi}{\alpha^2} \times \frac{(ct-L\cos\phi)}{\{(ct)^2+L^2-2Lct\cos\phi\}\,\{(ct)^2-L^2\}} \tag{22}$$

If the bistatic scattering strength is taken to be independent of bistatic angle then f=1 and Eq.(22) with the substitution of Eqs (11,12) is a closed-form solution for bistatic reverberation in a range-independent environment.

2.2.1 Bistatic scattering strength

This analytical approach can predict the effects of a known bistatic scattering law through the function $f(\beta)$ (see Eq. (7)). Referring to Eq. (19) we see that $\cos(\beta)$ is a simple function of ϕ,t and furthermore $f(\beta)$ is a simple multiplier of the reverberation. Therefore this approach can handle any functional form for f. Some possibilities are suggested below.

- $f(\beta) = 1 + a_1 \cos^2\beta$ (23)

This function has the same value for forward and back scatter with a bulge or sag at 90° depending on the value of the constant a_1.

- $f(\beta) = 1 + a_2 \cos\beta$ (24)

This function has a gradual change from forward to back scatter depending on the value of the constant a_2. The gradient of the function is continuous everywhere.

There are many other possibilities, for instance, making use of Eq. (16) and other trigonometric relationships we can form almost any shape including spikes or highlights.

- $f(\beta) = a_0 + a_1 \cos^n(\beta-\beta_0) = a_0 + a_1(b_1\cos\beta + b_2\sin\beta)^n$ (25)

2.2.2 Bistatic range-dependent reverberation

As noted earlier, the range-independent formulae can easily be converted to range-dependence by updating the P functions in Eq. (20) with the implicit propagation term in

Eq. (4.20) of [1], but we need to take some care with notation to distiguish between outgoing and incoming paths

$$P(r_s) = \frac{H_s}{\alpha H_{eff\_s} r_s^2} \{1 - \exp(-\theta_c^2 H_{c\_s}^2 \alpha r_s H_{eff\_s} / (2 H_{scat}^2 H_s^2))\} \tag{26}$$

$$P(r_r) = \frac{H_r}{\alpha H_{eff\_r} r_r^2} \{1 - \exp(-\theta_c^2 H_{c\_r}^2 \alpha r_r H_{eff\_r} / (2 H_{scat}^2 H_r^2))\} \tag{27}$$

H_s and H_r are the water depth at source and receiver, and H_{scat} is the water depth at the scatterer. There is a different effective depth along the path from the source H_{eff_s} and from the receiver H_{eff_r} to the same scatterer. Similarly the depth H_c that defines the steepest ray along the path is potentially different for source H_{c_s} and receiver H_{c_r} .

These equations have exactly the same form as before so the range-dependent version is

$$\begin{aligned} I_R(\phi, t) = (1 - \exp(-A_s r_s))(1 - \exp(-A_r r_r)) \frac{4c \mu f(\beta) \delta t \ \delta\phi H_s H_r}{\alpha^2 H_{eff\_s} H_{eff\_r}} \\ \times \frac{(ct - L\cos\phi)}{\{(ct)^2 + L^2 - 2Lct\cos\phi\}\{(ct)^2 - L^2\}} \end{aligned} \tag{28}$$

with

$$A_{s,r} = \alpha \theta_c^2 H_{c\_s,r}^2 H_{eff\_s,r} / (2 H_{scat}^2 H_{s,r}^2) \tag{29}$$

Note that this formula works for *any* slowly varying bathymetry, we simply need to be able to calculate the effective depth for each range through

$$H_{eff\_s,r}(r) = (H_{s,r}^2 H_{scat}^2 / r) \int_0^r \frac{dr'}{H^3(r')} \tag{30}$$

2.2.3 Tilted plane seabed

Let us define a bottom slope ε_o ($\varepsilon_o = \partial H / \partial y$) towards the North (at absolute bearing ψ = 0). Defining the receiver location as the horizontal origin we have

$$H_{scat} = H_r + r_r \varepsilon_o \cos\psi \tag{31}$$

The source is located at distance L and bearing ψ_o from the receiver, and so the depth at the source must be

$$H_s = H_r + L\,\varepsilon_o \cos\psi_o \tag{32}$$

The effective depths are given [4, 1] by

$$H_{eff\_s} = (H_s + H_{scat})/2 \tag{33}$$

$$H_{eff\_r} = (H_r + H_{scat})/2 \tag{34}$$

and because we have

$$H_{c\_s,r} = MIN(H_{s,r}, H_{scat}) \tag{35}$$

$$H_{s,r} H_{scat} / H_{c\_s,r} = MAX(H_{s,r}, H_{scat}) \tag{36}$$

the exponent coefficients are

$$A_s = \alpha\,\theta_c^{\,2}\,(H_s + H_{scat})/\{4(MAX(H_s, H_{scat}))^2\} \tag{37}$$

$$A_r = \alpha\,\theta_c^{\,2}\,(H_r + H_{scat})/\{4(MAX(H_r, H_{scat}))^2\} \tag{38}$$

Now all the terms in Eq. (28) can be written explicitly in terms of ϕ,t (or ψ,t, since ϕ is still measured relative to the source receiver axis, $\phi = \psi - \psi_o$). Taking them in turn, r_s, r_r are related to ϕ,t by Eqs (11,12); H_{scat} is defined by Eq. (31) in terms of r_r and ψ and therefore related to ϕ,t; and equally A_s, A_r and H_{eff_s}, H_{eff_r} are related to ϕ,t.

2.2.4 Tilted plane with shelf

A shelf can be introduced by simply modifying Eqs. (31-34). We retain the variables H_s, H_r and H_{scat} but introduce new ones that may be limited by the shelf depth H_{shelf}.

$$H'_s = MAX(H_s, H_{shelf}) \tag{39}$$

$$H'_r = MAX(H_r, H_{shelf}) \tag{40}$$

$$H'_{scat} = MAX(H_{scat}, H_{shelf}) \tag{41}$$

Taking the example of source on the slope with scatterer on the shelf we can use the definition of effective depth Eq. (30) to show that

$$H_{eff\_s} = \eta (H_s + H'_{scat}) / 2 + (1-\eta) H_s{}^2 / H'_{scat}{}^3 \tag{42}$$

where the coefficient η can be written conveniently in terms of depths rather than ranges

$$\eta = (H_s - H'_{scat}) / (H_s - H_{scat}) \tag{43}$$

2.2.5 Target echoes and other scattering laws

Target echoes and other scattering laws can be accommodated in the same way as all the above variants. For instance, the range-dependent equation for target propagation is (Eq. (4.13) [1], cf. Eq. (1) above)

$$P(r) = \sqrt{\frac{2\pi}{\alpha r^3 H_{eff}}} \operatorname{erf}\{\sqrt{\frac{\alpha\, r H_{eff}}{2}} \frac{\theta_c H_c}{H_r H_s}\} = \sqrt{\frac{2\pi}{\alpha r^3 H_{eff}}} \operatorname{erf}\{\sqrt{A\, r}\} \tag{44}$$

For a point target the solution is simply

$$I_T = P(r_s) P(r_r)\, S_T \tag{45}$$

Clearly this is again a function of r, H_{eff}, A with appropriate subscripts for incoming and outgoing paths for which we can still use Eqs. (33,34,37,38). Therefore after making the substitutions this constitutes a closed-form solution for a target.

For reverberation from point scatterers we return to Eq. (8) but the range dependence of P is slightly different so we find

$$\begin{aligned} I_B(\phi, t) = &\left(\operatorname{erf}\{\sqrt{A_s\, r_s}\}\right)\left(\operatorname{erf}\{\sqrt{A_r\, r_r}\}\right) \frac{\pi c \delta t\ \delta\phi}{\alpha}\, S_B \\ &\times \{(ct)^2 + L^2 - 2Lct\cos\phi\}\, \{(ct)^2 - L^2\}^{-1/2} \end{aligned} \tag{46}$$

2.2.6 Signal-to-reverberation-ratio (SRR)

Combining Eq.(28) with Eq. (45) we have an expression for the SRR.

$$\begin{aligned} \frac{I_T(\phi, t)}{I_R(\phi, t)} = &\frac{4\pi\alpha}{\mu f(\beta) c \delta t\ \delta\phi} \frac{\sqrt{H_{eff\_s}\, H_{eff\_r}}}{H_s\, H_r} \frac{\left(\operatorname{erf}(\sqrt{A_s\, r_s})\right)\left(\operatorname{erf}(\sqrt{A_r\, r_r})\right)}{\left(1-\exp(-A_s\, r_s)\right)\left(1-\exp(-A_r\, r_r)\right)} \\ &\times \frac{(ct - L\cos\phi)^2}{\sqrt{\{(ct)^2 + L^2 - 2Lct\cos\phi\}\, \{(ct)^2 - L^2\}}} \end{aligned} \tag{47}$$

There are two varieties of long range and either could be separately important. One is when $r >> A^{-1}$ (the gaussian angle spread is narrower than the critical angle) and the other is when $r >> L$ (bistatic is indistinguishable from monostatic). The first limit alone results in

$$\frac{I_T(\phi,t)}{I_R(\phi,t)} = \frac{4\pi\alpha}{\mu f(\beta) c\delta t\ \delta\phi} \frac{\sqrt{H_{eff\_s} H_{eff\_r}}}{H_s H_r} \times \frac{(ct - L\cos\phi)^2}{\sqrt{\{(ct)^2 + L^2 - 2Lct\cos\phi\}\{(ct)^2 - L^2\}}} \tag{48}$$

The second limit alone is

$$\frac{I_T(\phi,t)}{I_R(\phi,t)} = \frac{4\pi\alpha}{\mu f(\beta) c\delta t\ \delta\phi} \frac{H_{eff}}{H_s H_r} \frac{\left(\mathrm{erf}(\sqrt{A_s r_s})\right)\left(\mathrm{erf}(\sqrt{A_r r_r})\right)}{\left(1-\exp(-A_s r_s)\right)\left(1-\exp(-A_r r_r)\right)} \tag{49}$$

where the effective depths along the two paths are now indistinguishable.

Beyond both limits we have

$$\frac{I_T(\phi,t)}{I_R(\phi,t)} = \frac{4\pi\alpha}{\mu f(\beta) c\delta t\ \delta\phi} \frac{H_{eff}}{H_s H_r} \tag{50}$$

and this is identical to the formula in [1] except for the fact that H_s^2 is replaced by $H_s H_r$.

3
Examples in an analytical environment

In this section we show some graphical examples of the above formulae. The way the equations have been written, assuming a given ϕ,t means that plots of intensity in bearing-time space are straightforward. We can also construct plots in horizontal plan or map format showing source and receiver superimposed on the bathymetry. To do this, however, it is most convenient to start with the x,y coordinates of each scatterer (the pixel to be plotted). Given the source and receiver position we can then calculate the ranges r_s, r_r and the travel time and bearing, whence we continue as usual.

In all figures the bottom reflection properties are: reflection loss gradient α_{dB} = 1 dB/radian and critical angle θ_c = 30°. Note that in the calculation of reverberation and target echo there are several quantities that are simple multipliers. For reverberation the multiplier is $c\delta t\ \delta\phi\ \mu$ (Eq. 28), and for target it is S_T (Eq. 45). In all the plots we have assumed these to be

$c\delta t$ = 1500×0.01 = 15m (10ms pulse length)

$\delta\phi$ = 1/60 = 0.0167 radians (1° beam)

$\mu = 10^{-27/10}$

S_T = 10 dB

Similarly for clarity we have assumed a source level of SL = 0dB. The pulse length δt is the inverse of the bandwidth and corresponds to the correlation time in the case of a correlation sonar. The reverberation level, target echo and source level can be regarded as spectral levels or levels in the band.

In this way the figures are representations of the formulae as they stand. A conversion to other values can be made by altering the quantities SL+10 log($c\delta t\ \delta\phi\ \mu$) for reverberation, SL+10 log(S_T) for target, or 10 log(S_T / $c\delta t\ \delta\phi\ \mu$) for SRR. Of course, it is a simple matter to add gains, detection thresholds, etc., as desired.

3.1 Range-independent; Lambert; f=1.

In Fig. 3 water depth is a uniform 200 m and source/receiver separation is 20 km. Fig. 3(a) is a radar-type map projection showing strong reverberation from forward scattering in the area between the source (at 0,20) and receiver (at 0,0). The reverberation is

symmetrical about the baseline but asymmetrical about the perpendicular bisector. This is because the intensity for each round trip delay time and bearing *at the receiver* (Fig 3(b)) is mapped into x,y; this operation is not symmetrical with respect to the source and receiver position. Figure 3(c) shows the target echo strength for a 'probe' target at all conceivable positions. It resembles the 'ovals of Cassini' which would have been obtained for inverse power law propagation. Finally Fig. 3(d) shows that the SRR has a large area of poor performance between source and receiver and a small area of good performance just behind the receiver. Otherwise the SRR is relatively flat and the values of SRR = $(4S_T\pi\alpha)/(H\mu\,\delta\phi\,c\delta\tau)$ = 24.6 dB are close to those for monostatic long range predicted by the tables in [1]. At first sight the absolute magnitude of the SRR looks rather high, but this is a simple consequence of Lambert's law. In contrast an angle-independent scatterer with scattering strength $S_B = \mu$ and *any propagation law* has SRR = $8S_T/(r\mu\,\delta\phi\,c\delta\tau)$ = 12.0 dB at 10 km and only 5.0 dB at 50 km.

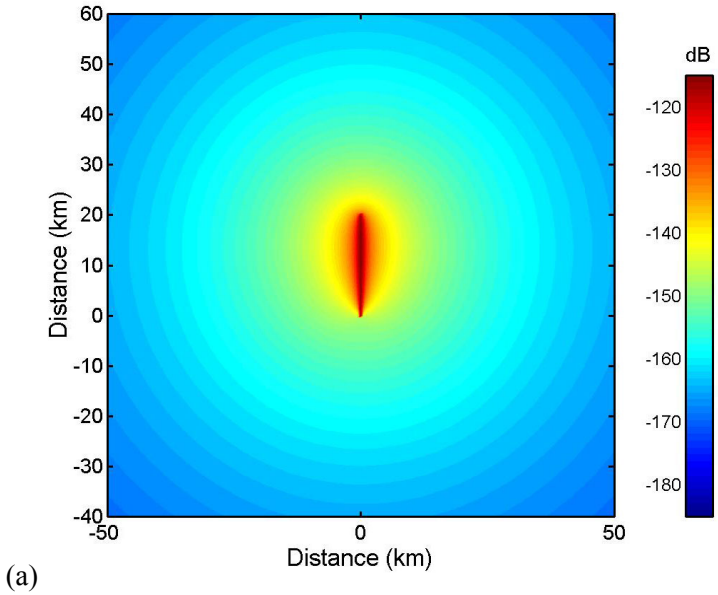

(a)

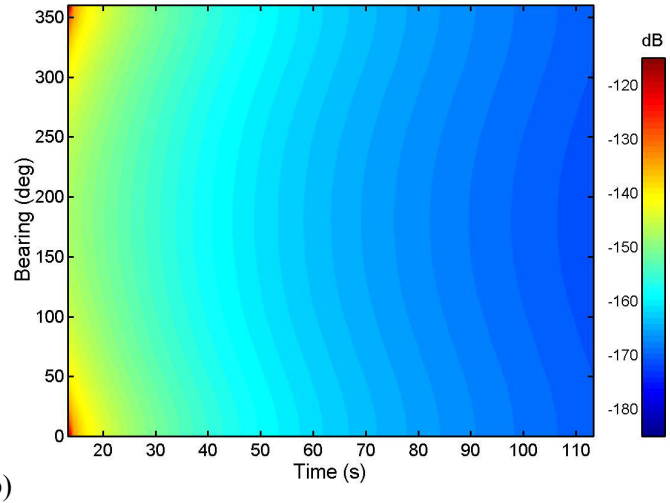

(b)

Figure 3 (continued on next page) Range-independent environment; source to north, (a) reverberation map, (b) reveberation bearing-time plot.

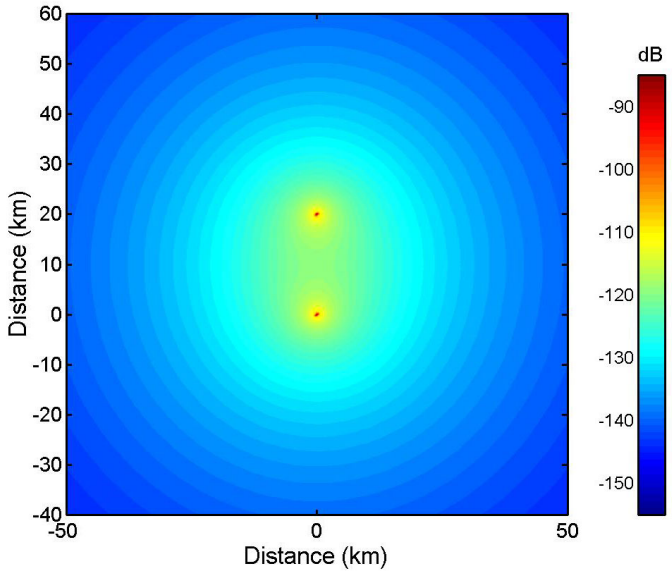

(c)

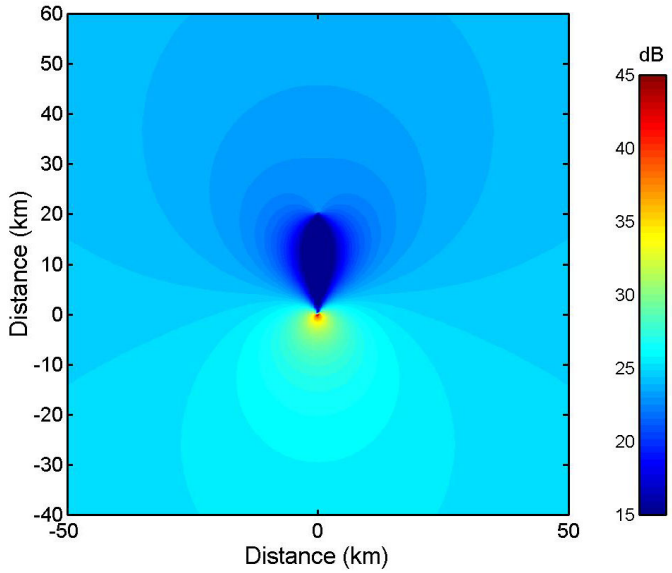

(d)

Figure 3 (continued) *Range-independent environment; source to north, (c) target echo map, (d) SRR map.*

3.2 Range-independent; Lambert; $f(\beta) = a+(1-a)\cos^2(\beta/2)$.

Figure 4 shows the effect of including a Lambert's law with varying bistatic angle dependence. The example is otherwise the same as Fig. 3. The bistatic angle dependence is

$$f(\beta) = a + (1-a)\cos^2(\beta/2)$$

with the coefficient a being 0.1 in Fig. 4(a,b) and 0.01 in Fig. 4(c,d). When $\beta = 0$ (back scatter) $f = 1$, but when $\beta = \pi$ (forward scatter) $f = a$. Thus forward scatter is 10 dB weaker than backscatter in the first case and 20 dB weaker in the second. Nevertheless we only expect to see differences from Fig. 3 at short ranges since at long range there is no distinction between bistatic and monostatic and there is only back scattering. In particular we expect to see differences in the area between the source and receiver. On the baseline itself even weak scatterers continue to contribute strongly because they all arrive at the same time. Mathematically the first arrival is a singularity if, as in this approximation, the source and receiver are in the plane of the scatterers. An interesting aside is that one could investigate the bistatic angle dependence of scattering surfaces experimentally by comparing the shape of the measured intensity contours with these theoretical ones.

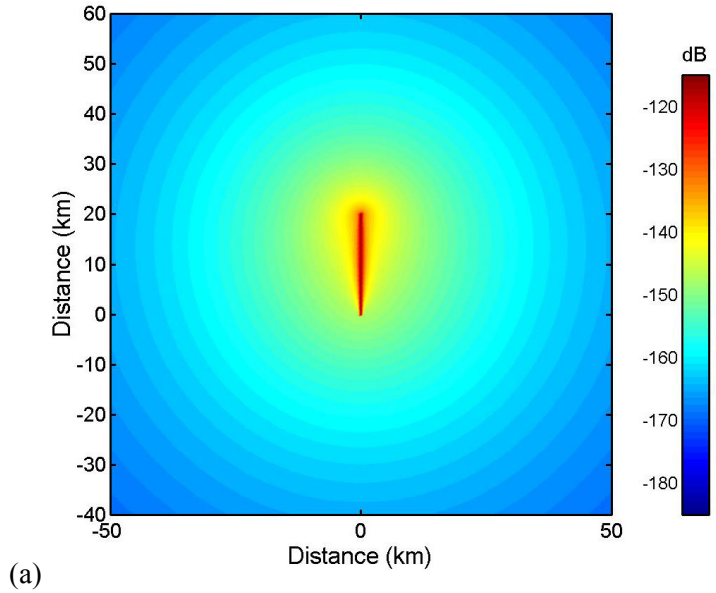

(a)

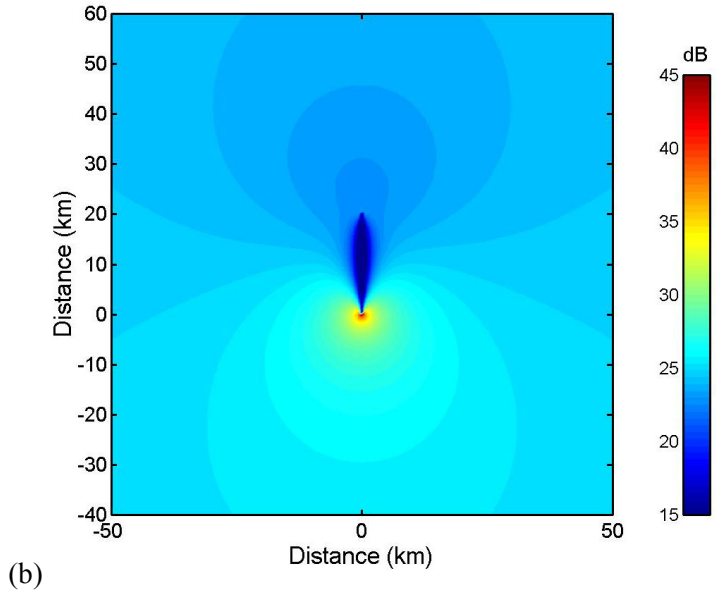

(b)

Figure 4 (continued on next page) *Effect of scattering law dependence on bistatic angle. Range-independent environment; source to north, (a) reverberation (b) SRR, both with forward scatter10dB less than back scatter.*

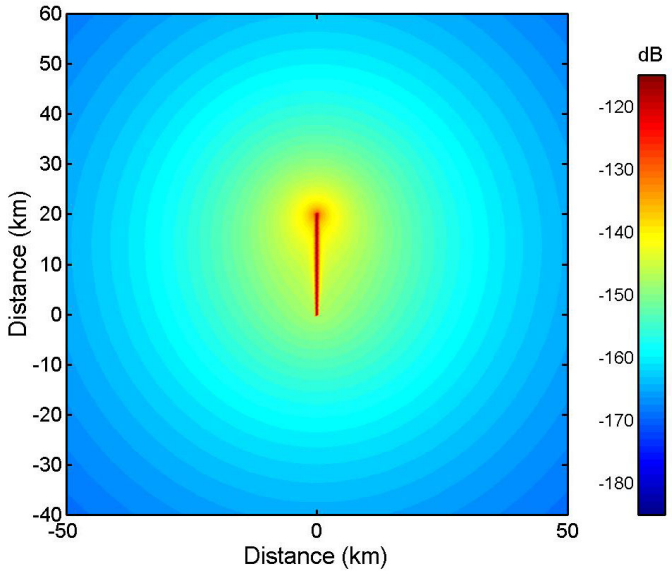

(c)

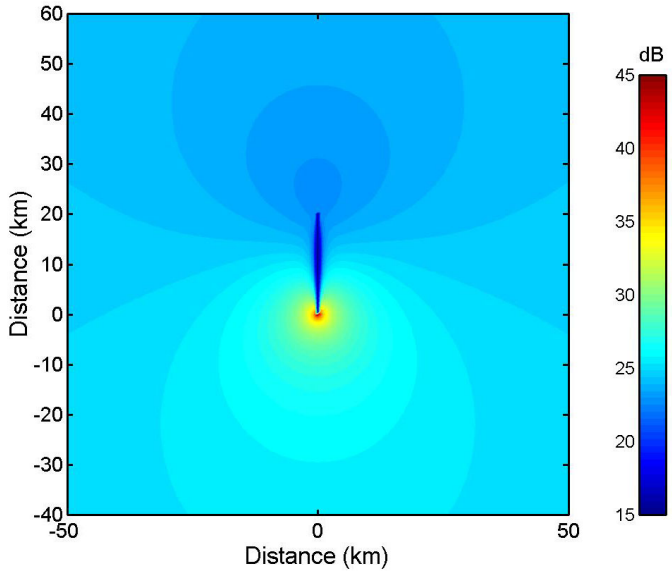

(d)

Figure 4 (continued) *Effect of scattering law dependence on bistatic angle. Range-independent environment; source to north, (c) reverberation (d) SRR, both with forward scatter20dB less than backscatter.*

3.3 Source and receiver on a slope; Lambert; f=1.

Figure 5 shows a receiver in 600 m of water at (0,0) looking obliquely (120°) up a bottom slope of 0.01 towards a source 20 km away in 500 m of water. The reverberation is slightly stronger upslope than down slope. The bearing-time plot (Fig. 5(b)), because it happens to see further into the distance, shows an additional feature at 180° (deep blue). This is the range at which we reach zero water depth. Combining the reverberation with the innocuous looking target echo we find a highly asymmetrical SRR plot in Fig. 5 (d). Otherwise there are still the two features found before, namely, poor performance between source and receiver and good performance just behind the receiver.

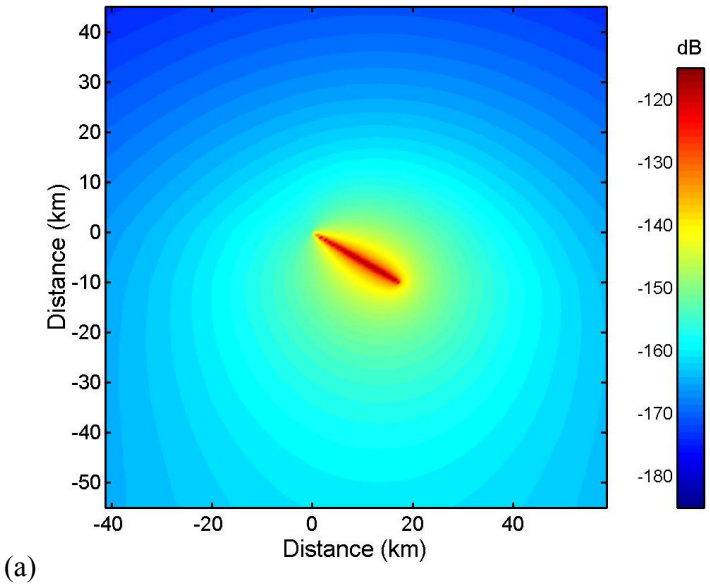

(a)

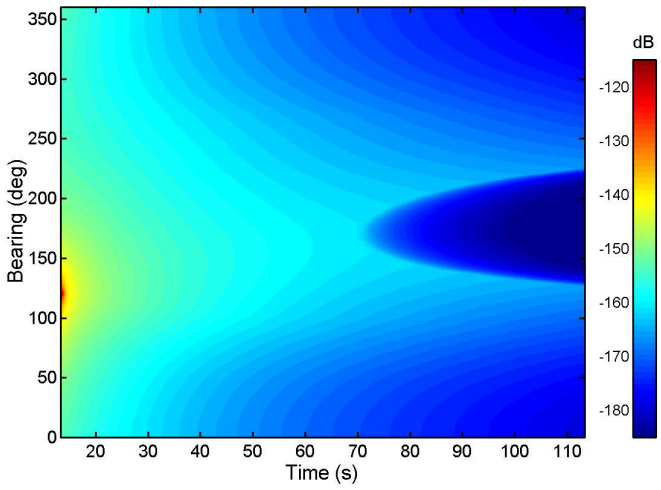

(b)

Figure 5 (continued on next page) *Source and receiver on a slope,(f=1) (a) reverberation map, (b) reverberation bearing-time plot.*

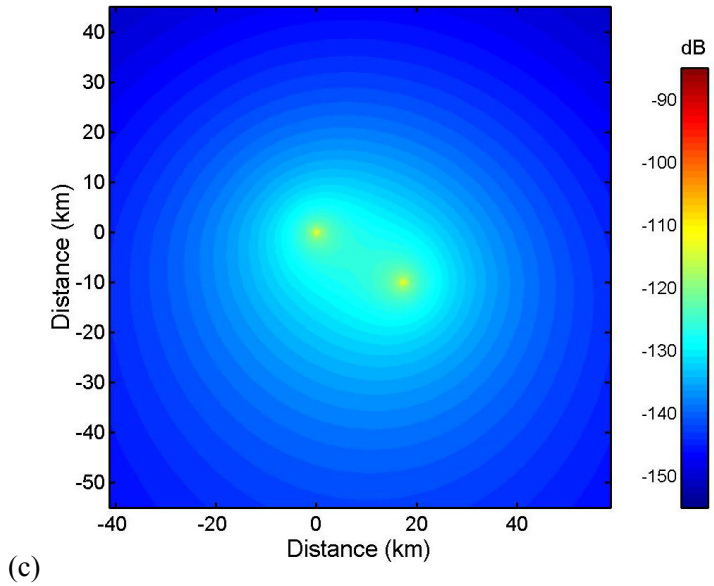

(c)

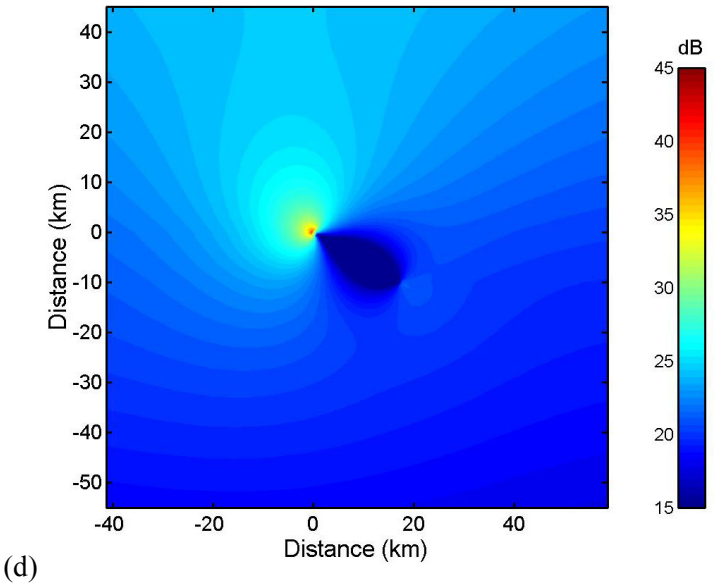

(d)

Figure 5 (continued) *Source and receiver on a slope,(f=1), (c) target echo map, (d) SRR map.*

3.4 Source and receiver on a slope near a shelf; Lambert; f=1.

Moving the receiver and source up the slope to 200 m water depth (the coordinate system is centred on the receiver) and introducing a shelf of 30 m 17 km to the south Fig. 6 shows an even more distorted result. Another interesting feature is the 'wings' seen in

Figs. 6(a,b). Note that in the long range limit as the water shallows reverberation is unaffected but the target echo and therefore SRR are enhanced. It is interesting to compare these plots with the equivalent monostatic ones shown in Fig. 7.

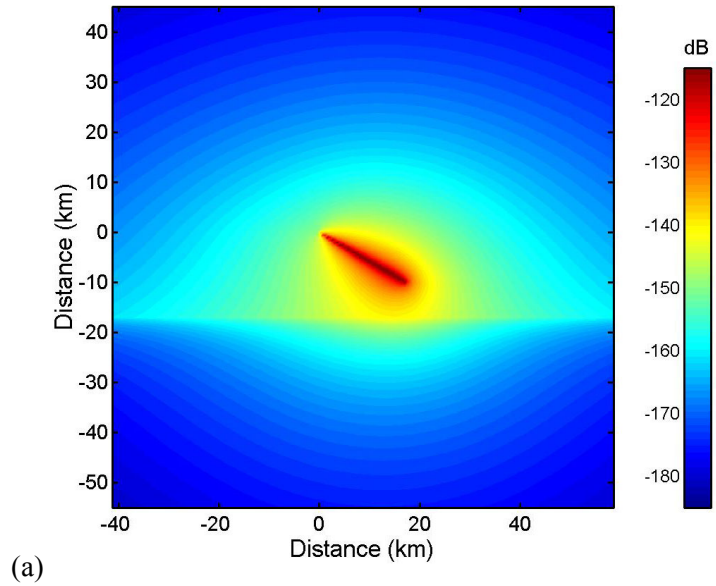

(a)

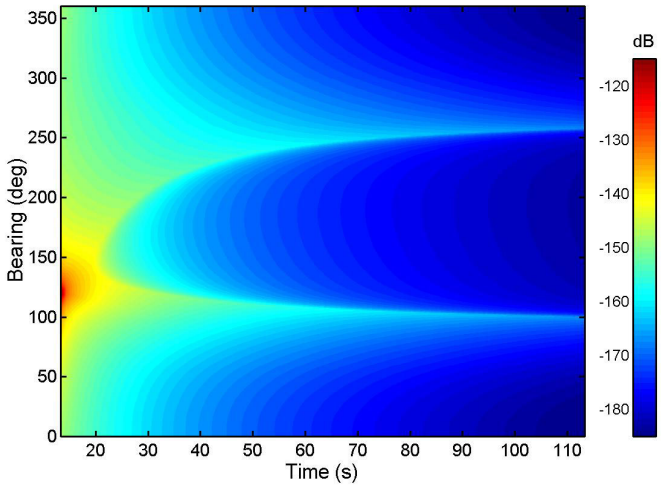

(b)

Figure 6 (continued on next page) *Source and receiver on a slope near a shelf, (f=1) (a) reverberation map, (b) reverberation bearing-time plot.*

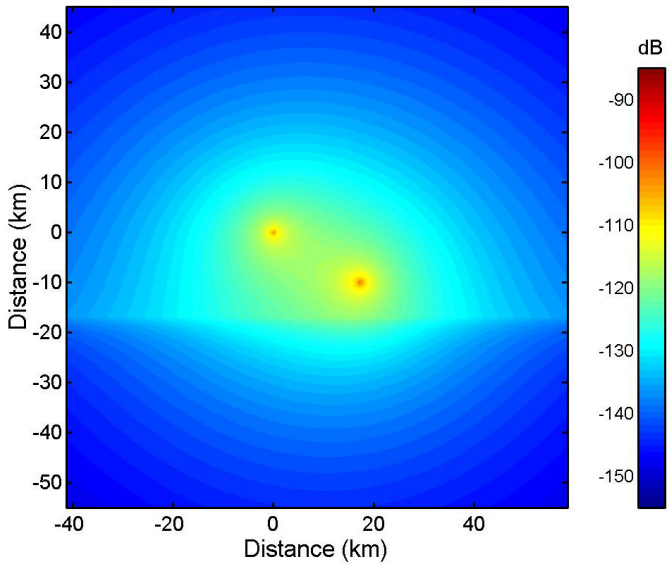

(c)

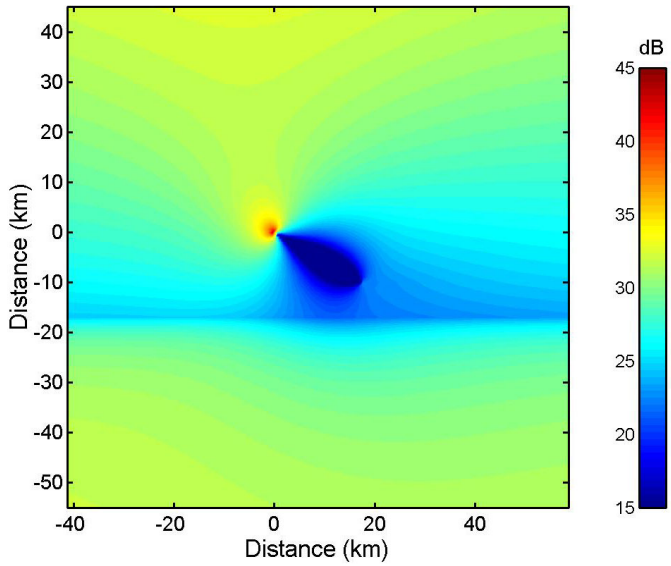

(d)

Figure 6 (continued) *Source and receiver on a slope near a shelf, (f=1), (c) target echo map, (d) SRR map.*

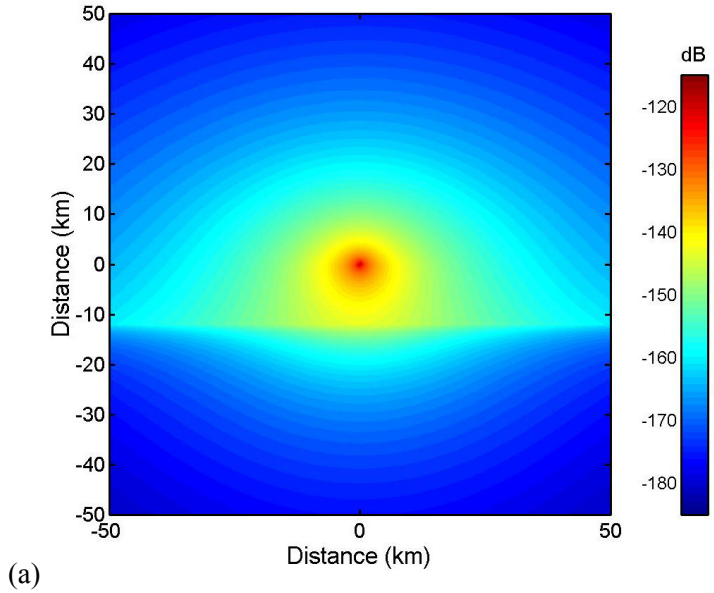

(a)

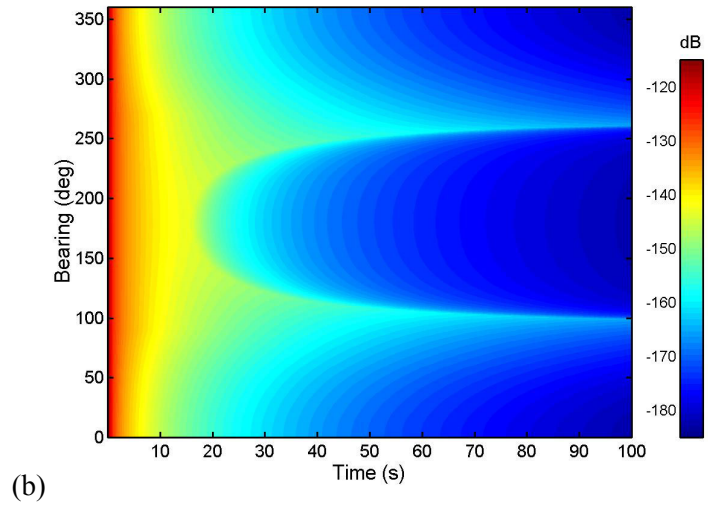

(b)

Figure 7 (continued on next page) *Monostatic sonar on a slope near a shelf, (f=1) (a) reverberation map, (b) reverberation bearing-time plot.*

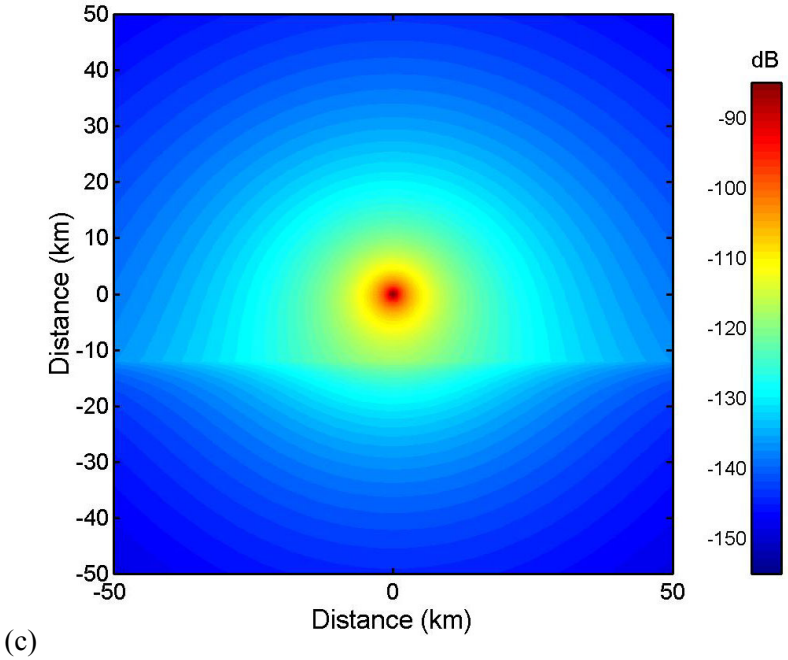

(c)

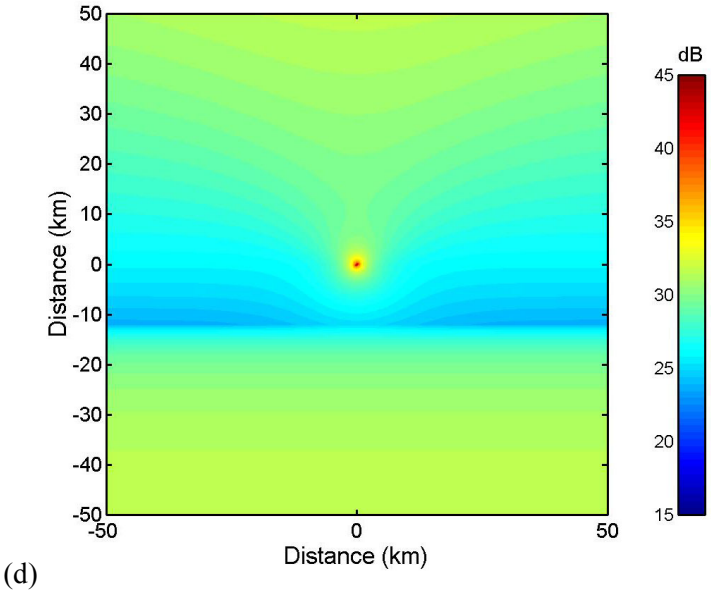

(d)

Figure 7 (continued) *Monostatic sonar on a slope near a shelf,(f=1) (c) target echo map, (d) SRR map.*

3.5 Receiver on a slope; source on a shelf; Lambert; f=1.

In Fig. 8 the source and receiver straddle the shelf edge. The receiver is in 80 m of water and the source is on the 30 m shelf. We now find that the SRR is about 10 dB higher on the downslope side than on the shelf side. This is because it depends on the effective depth which is about 30 m at the beginning of the shelf and several hundred metres on the slope.

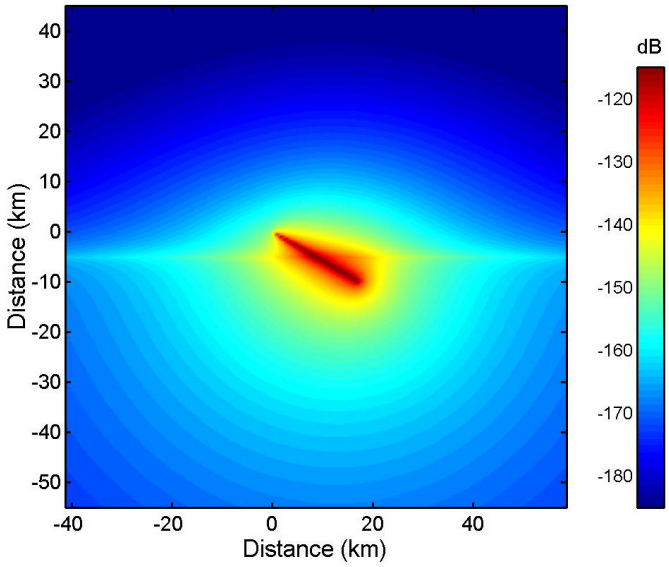

(a)

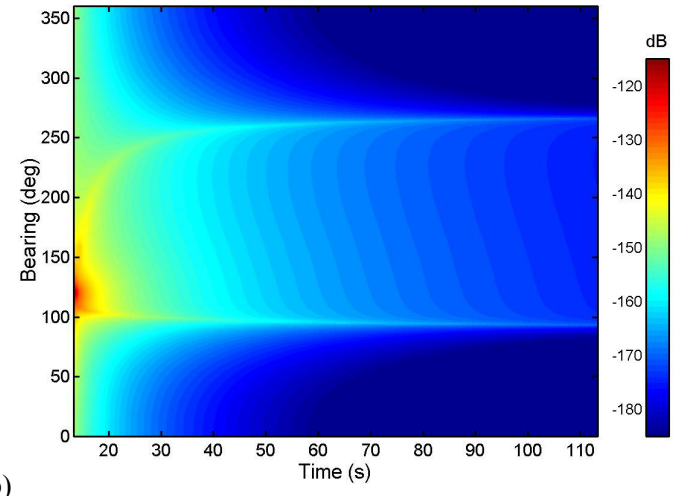

(b)

Figure 8 (continued on next page) *Receiver on a slope source on a shelf, (f=1) (a) reverberation map, (b) reverberation bearing-time plot.*

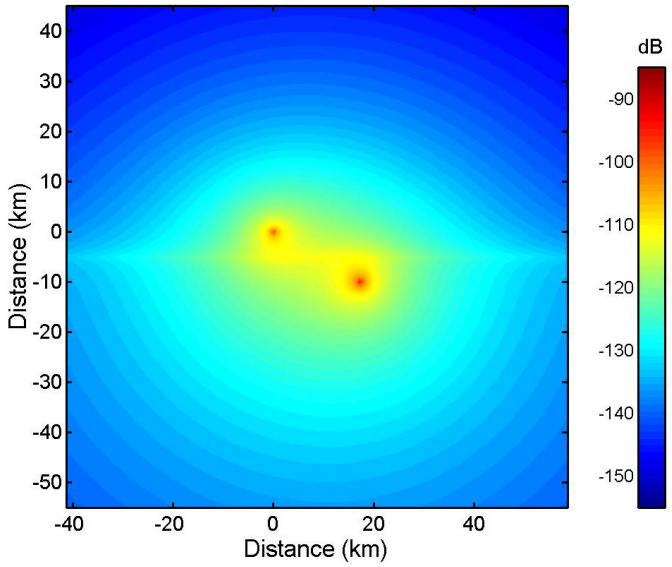

(c)

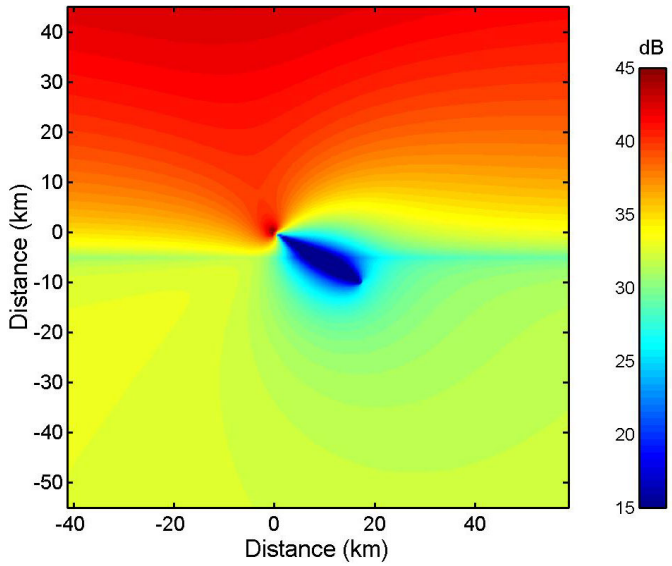

(d)

Figure 8 (continued) *Receiver on a slope source on a shelf, (f=1), (c) target echo map, (d) SRR map.*

3.6 Source on a slope, receiver on a shelf; Lambert; f=1.

Figure 9 shows the same geometry as Fig. 8 but with the source and receiver exchanged. There are subtle differences in the vicinity of the source and receiver as might be expected from earlier findings, but otherwise the plots are more or less the same.

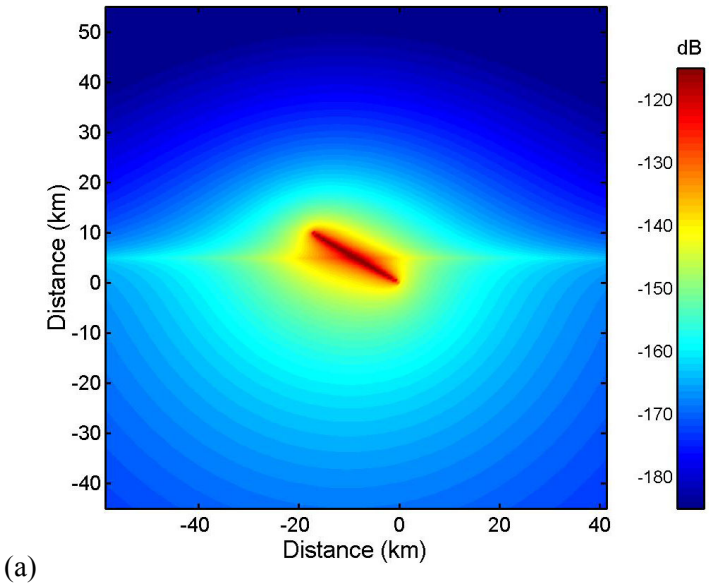

(a)

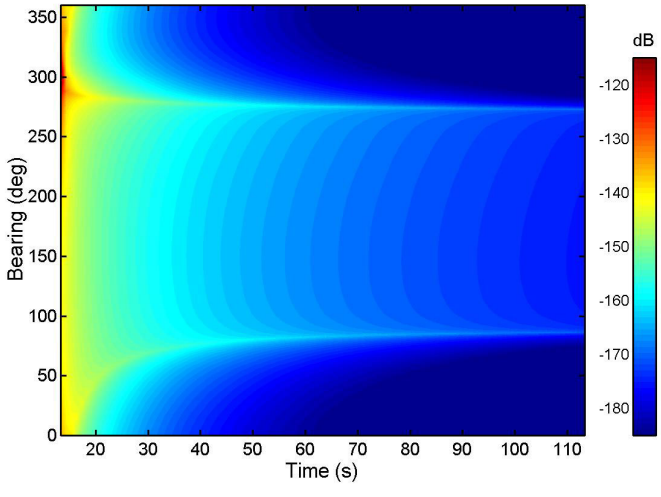

(b)

Figure 9 (continued on next page) *Source on a slope receiver on a shelf, (f=1) (a) reverberation map, (b) reverberation bearing-time plot.*

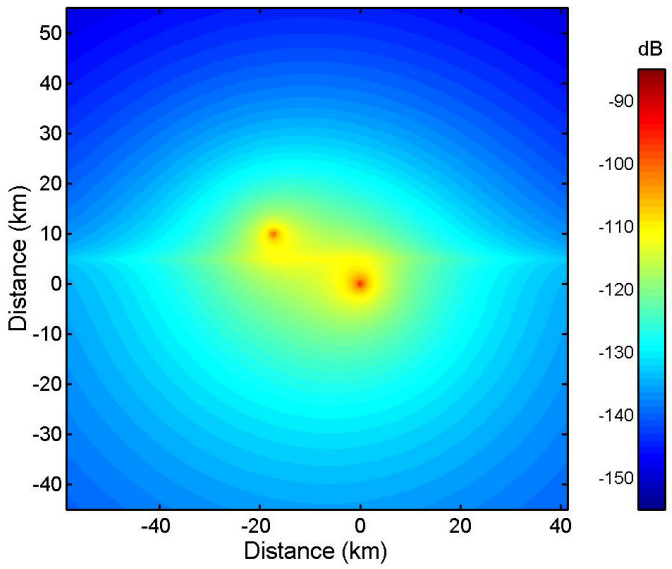

(c)

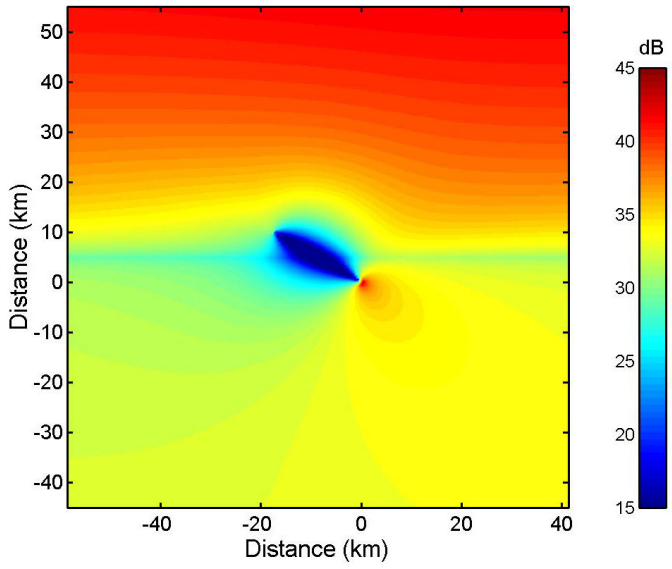

(d)

Figure 9 (continued) *Source on a slope receiver on a shelf, (f=1), (c) target echo map, (d) SRR map.*

3.7 Source and receiver on a shelf near a slope; Lambert; f=1.

In Fig. 10 both source and receiver have moved on to the shelf and one can see the very weak reverberation still coming from the deep water beyond the shelf. The SRR on the shelf is more or less the same as in Fig. 9, but interestingly there is very good SRR towards deep water where reverberation is weak.

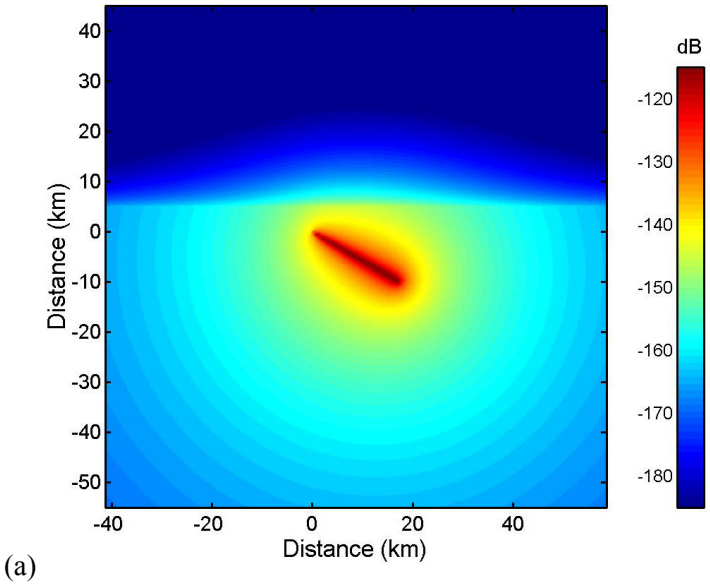

(a)

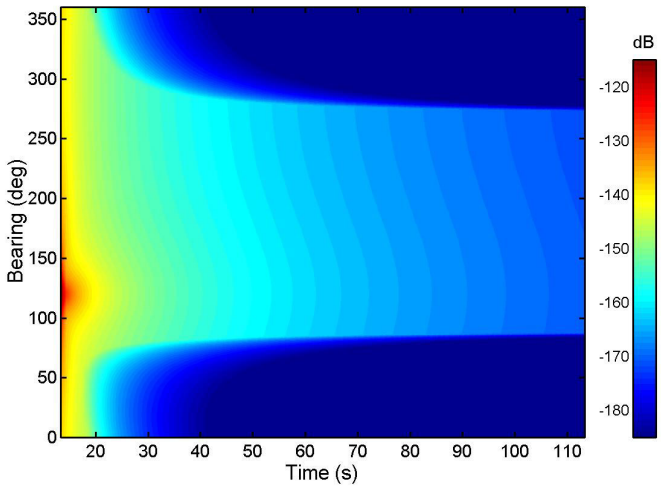

(b)

Figure 10 (continued on next page) *Source and receiver on a shelf near a slope, (f=1) (a) reverberation map, (b) reverberation bearing-time plot.*

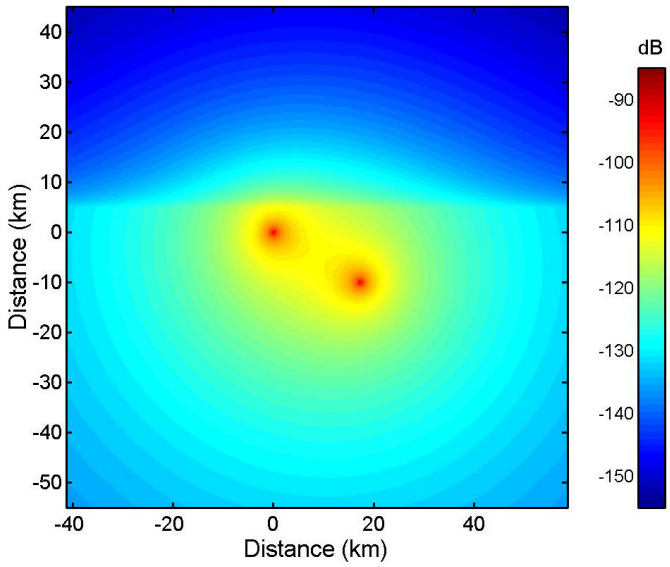

(c)

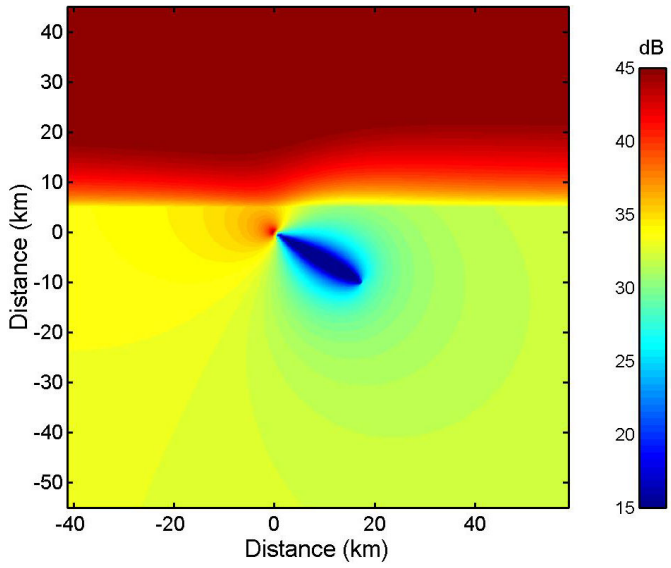

(d)

Figure 10 (continued) *Source and receiver on a shelf near a slope, (f=1), (c) target echo map, (d) SRR map.*

4

Examples in a gridded environment

Whilst still retaining the analytical form of the equations it is possible also to produce solutions for gridded data. Here we show examples in a bathymetric grid, however almost every one of the parameters considered so far could be gridded with no further computational effort. For instance one could include in gridded form the environmental parameters: H, α, θ_c, μ, and the coefficients of $f(\beta)$. It is also possible to grid some of the target parameters such as its orientation, aspect angle and bistatic angle behaviour.

The formulae Eqs. (28-30, 44-45) are general so, as long as we know H_{eff} and H_c from source and receiver to every scatterer it is possible to calculate reverberation and target echo. This we do numerically by using Eq.(30) for H_{eff} and by finding the outward cumulative minimum depth for H_c. Thus we start with a rectangular depth grid then, separately for source and receiver, we set up a small number of radials with regular range steps. At each of these points we interpolate the water depth and form a complete set of H_{eff} and H_c. We then interpolate these values back into the original rectangular grid. This is all that is required to evaluate Eqs. (28, 45).

4.1 Gaussian seamount

First we take a simple example of a numerically generated, 20 km half-width gaussian seamount rising from a 200m deep plane to a 30m peak centred at (0,10). In Fig. 11 the gaussian's depth contours are shown as black lines. The receiver is at (0,-45) and the source is at range 40 km bearing 60°. In Fig. 11(a) there is strong reverberation from the front face of the seamount and a pronounced shadow behind. A similar but slightly weaker effect is seen with the target echo in Fig. 11(b). The consequence in Fig. 11(c) is poor performance in front of the seamount but very good performance behind. This paradoxical behaviour is caused by the very weak reverberation but not quite so weak target echo. In reality this would be possible with a loud enough source or weak enough noise. If we include a noise level the result is as shown in Fig. 11(d). The noise level used in this case is SL-180 dB.

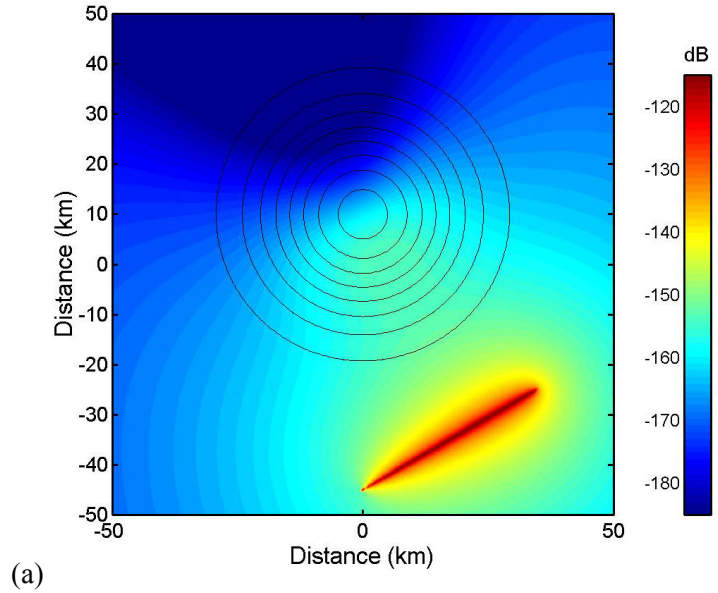

(a)

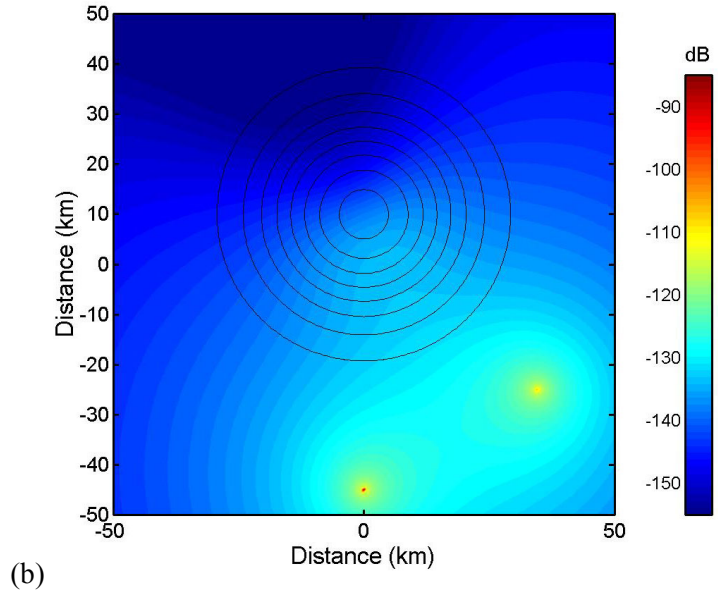

(b)

Figure 11 (continued on next page) *Source and receiver near a gaussian seamount, (f=1) (a) reverberation map, (b) target echo map.*

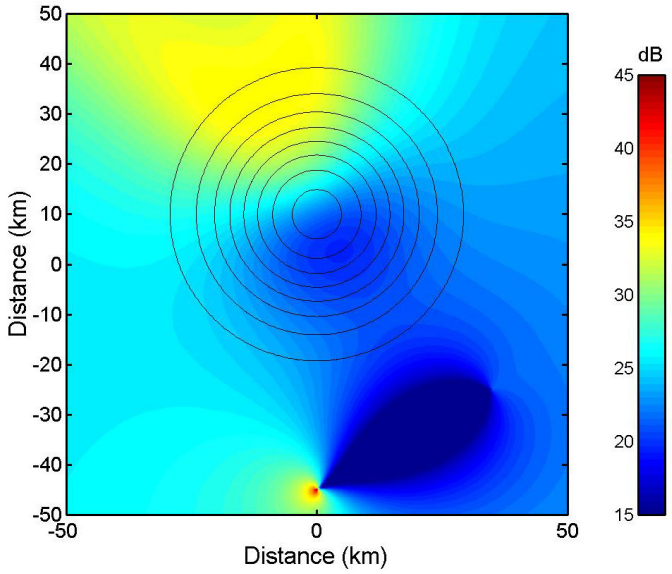

(c)

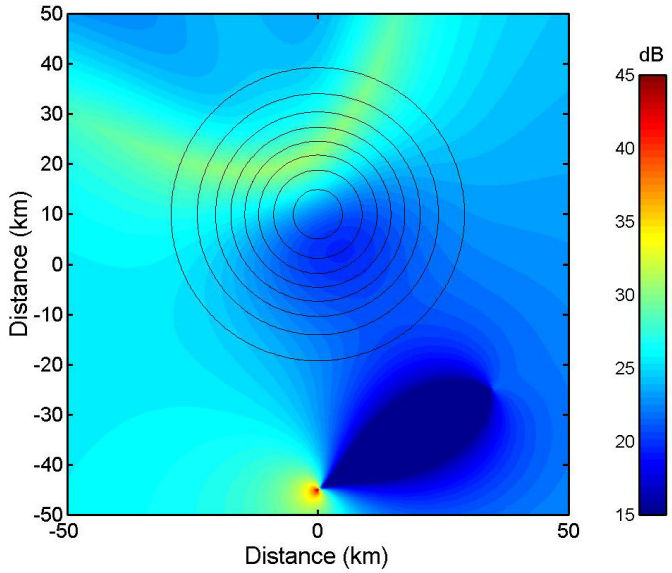

(d)

Figure 11 (continued) *Source and receiver near a gaussian seamount, (f=1) (c) SRR map, (d) SRR map modified by addition of noise.*

4.2 Real bathymetry south of Sicily near the Ragusa Ridge

An example using a bathymetric database is shown in Fig. 12. The area is the Malta Plateau south of Sicily with Malta visible at bottom left and Ragusa Ridge on the right. The coastline is shown in red. The receiver is at (20,-5) 118 m of water and the source is 20 km away at (9.54,0.2) in 177 m of water. Again we see the strongest reverberation from the shallow water and slopes near land. We can see most clearly in the SRR plot that the coastline produces a straight edged shadow aligned with either source or receiver (both paths are necessary). Again we see good performance in the deep water on either side of the ridge, but in practice this would be spoilt by the presence of noise. In Fig. 13 we have exchanged source and receiver. There are minor differences as we already expect.

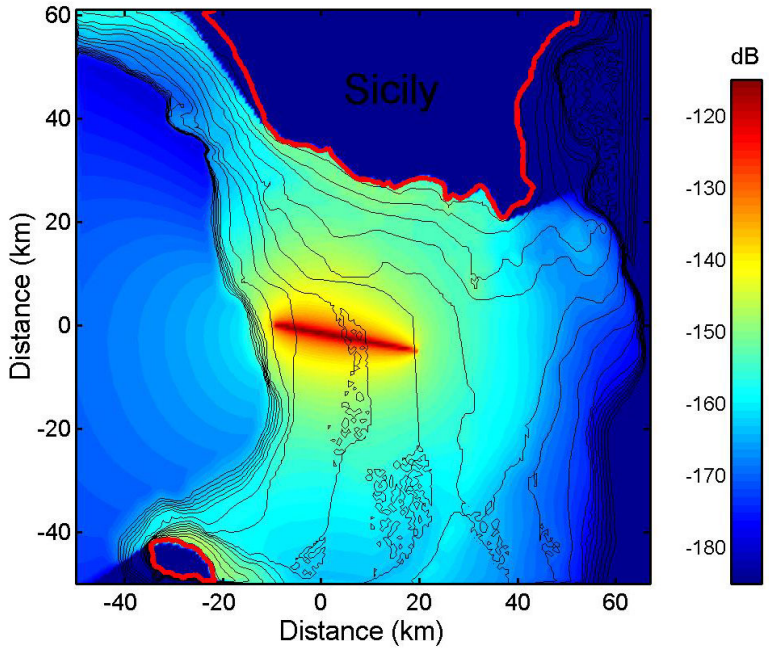

(a)

Figure 12 (continued on next page) *Source and receiver near the Ragusa Ridge, (f=1) (a) reverberation map.*

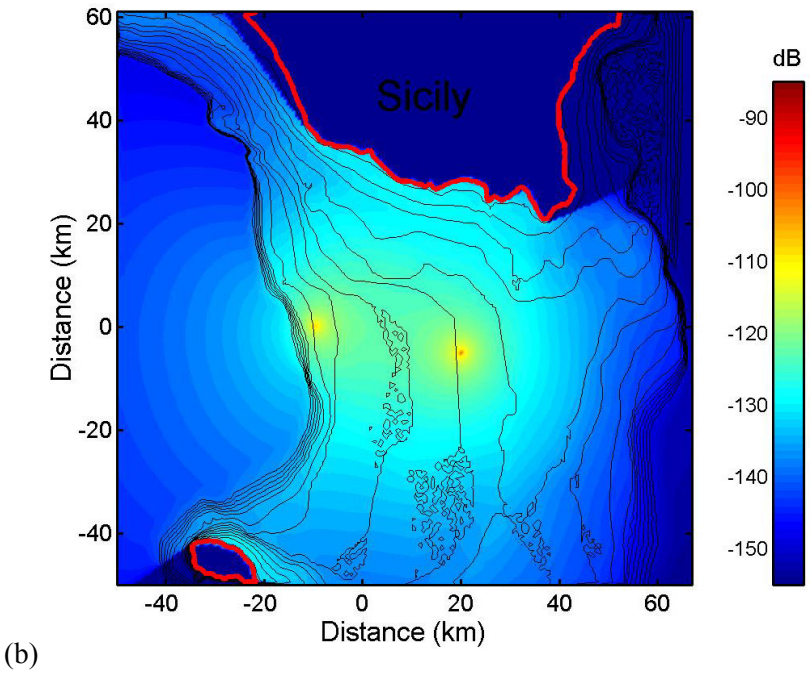

(b)

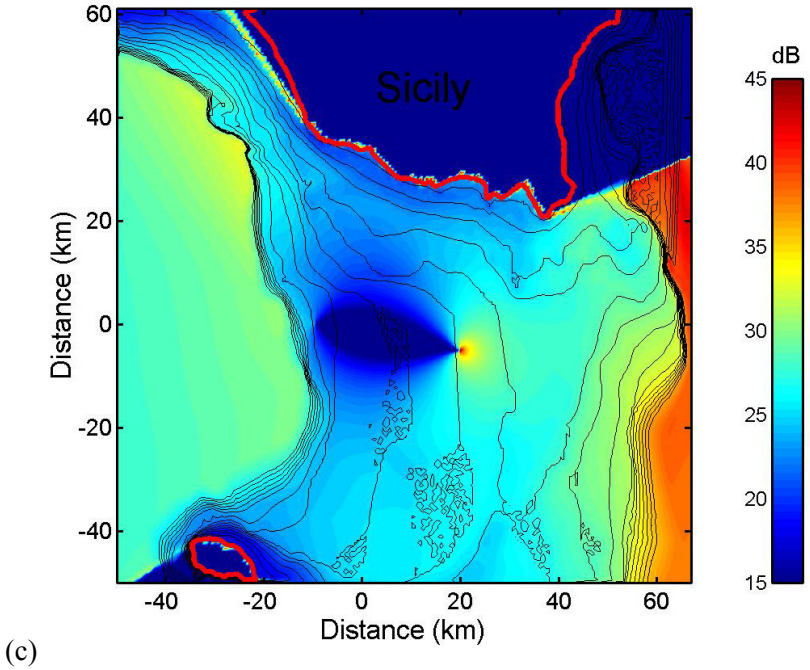

(c)

Figure 12 (continued) *Source and receiver near the Ragusa Ridge, (f=1), (b) target echo map, (c) SRR map.*

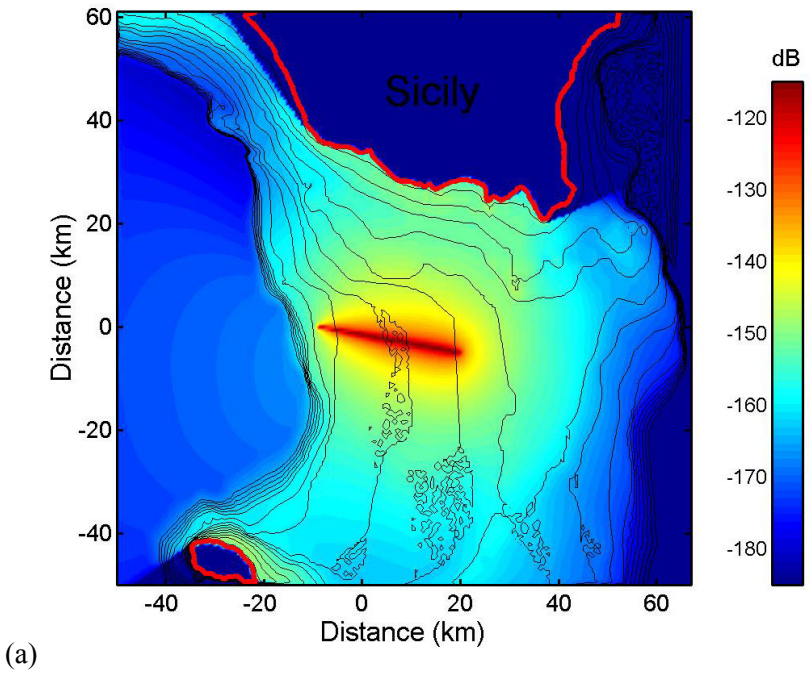

(a)

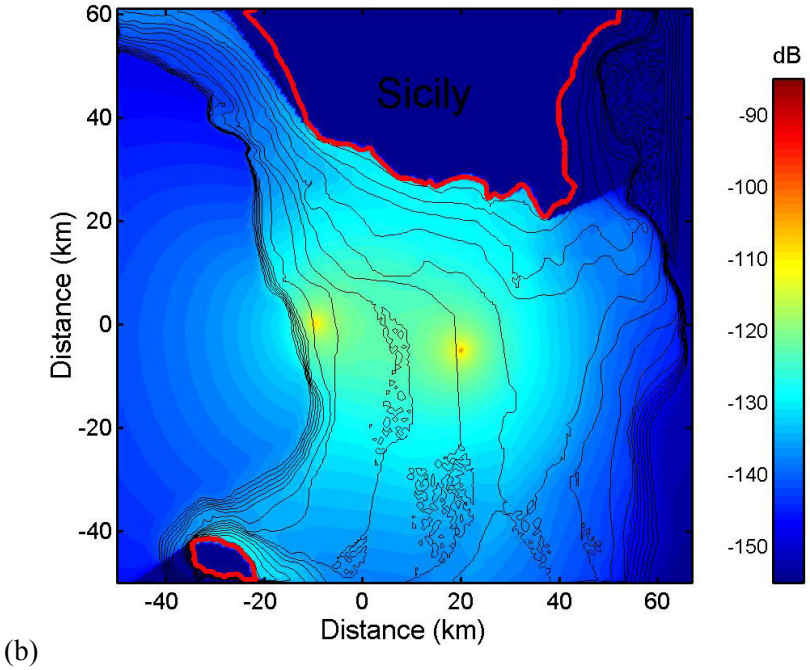

(b)

Figure 13 (continued on next page) *Swapped source and receiver near the Ragusa Ridge, (f=1) (a) reverberation map, (b) target echo map.*

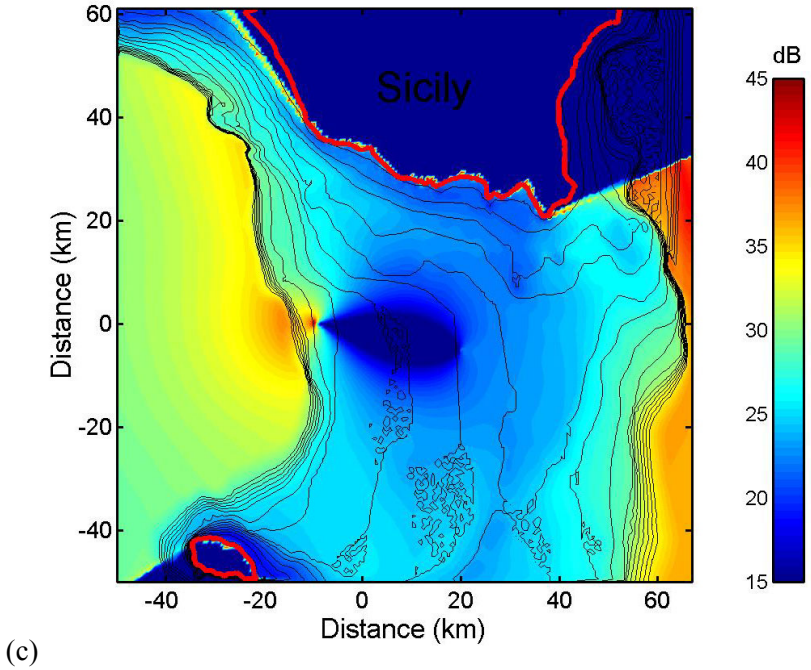

(c)

Figure 13 (continued) *Swapped source and receiver near the Ragusa Ridge, (f=1), (c) SRR map.*

5
Conclusions

Analytical formulae have already been derived for monostatic reverberation, target echo and signal-to-reverberation-ratio. This report has extended the approach to bistatic sonar. Here we have shown some examples of bistatic solutions in isovelocity environments although refracting environments can also be handled. A truly closed-form solution was given for a bistatic sonar in the vicinity of a shelf edge at the top of a slope. Graphical demonstrations of these formulae take about one second to run on a PC. Some of these examples reiterate the findings of the simple range-independent formulae, namely that target and reverberation follow the same range law at long range and therefore give a constant (range-independent) SRR (signal-to-reverberation-ratio).

The analytical solutions are written in terms of an effective depth and a cumulative minimum depth along the respective radials from source and receiver to each scatterer. Because of this it is possible to use the same approach by calculating these quantities numerically for each scatterer position. This quasi-analytical solution typically takes six seconds to run and can be applied to real bathymetry or arbitrary computer generated bathymetry.

Already one can see some interesting points in the examples, particularly the SRR plots. For a simple point target there is always extremely poor performance in the area between source and receiver. Conversely, performance is good behind the receiver. Usually facing slopes (upslope from target and receiver) give strong target echoes but stronger reverberation and therefore degraded performance. Surprisingly the reverberation shadow behind ridges is matched by a target echo shadow, and provided noise is relatively weak there will be detection opportunities.

References

[1] Harrison, C.H. Signal and reverberation with mode-stripping and Lambert's Law, SACLANTCEN SR-356. La Spezia, Italy, NATO SACLANT Undersea Research Centre, 2002.

[2] Harrison, C.H, Signal and reverberation formulas including refraction, SACLANTCEN SR-370. La Spezia, Italy, NATO SACLANT Undersea Research Centre, 2002.

[3] Harrison, C.H. Formulae for signal and reverberation with variable bathymetry and refraction, SACLANTCEN SM-358. La Spezia, Italy, NATO SACLANT Undersea Research Centre, 2002.

[4] Weston, D.E. Propagation in water with uniform sound velocity but variable-depth lossy bottom. *Journal of Sound and Vibration*, **47**, 1976:473-483.

Report no. changed (Mar 2006): SR-371-UU

Document Data Sheet

Security Classification		Project No.
		04-E
Document Serial No.	**Date of Issue**	**Total Pages**
SR-371	November 2002	44 pp.

Author(s)

Harrison, C.H.

Title

Formulae for bistatic signal and reverberation.

Abstract

This report demonstrates that it is possible to obtain closed-form solutions for signal and reverberation in a wide variety of bistatic scenarios including ducts and bottom bathymetry. These formulae adapt earlier monostatic solutions [SACLANTCEN Reports SR-356, SR-370, SM-358]. Examples are given for bistatic reverberation with the source and receiver near a shelf at the top of a slope. Results are presented both mathematically and graphically as plots of reverberation *vs* delay time and bearing and reverberation in map projection

Keywords

Reverberation – SRR – bistatic – bottom slope

Issuing Organization

North Atlantic Treaty Organization
SACLANT Undersea Research Centre
Viale San Bartolomeo 400, 19138 La Spezia, Italy

[From N. America: SACLANTCEN (New York) APO AE 09613]

Tel: +39 0187 527 361
Fax:+39 0187 527 700

E-mail: library@saclantc.nato.int